Hunkapiller, M. W., Hewick, R. M., Dreyer, W. J., & Hood, L. E. (1983) *Methods Enzymol. 91*, 399–413.
Jack, A., & Levitt, M. (1978) *Acta Crystallogr., Sect. A: Cryst. Phys., Diffr., Theor. Gen. Crystallogr. A34*, 931–935.
Jones, T. A., & Thirup, S. (1986) *EMBO J. 5*, 819–822.
Jurnak, F. (1985) *Science (Washington, D.C.) 230*, 32–36.
Kohno, K., Uchida, T., Ohkubo, H., Nakanishi, S., Nakanishi, T., Fukui, T., Ohtsuka, E., Ikehara, M., & Okada, Y. (1986) *Proc. Natl. Acad. Sci. U.S.A. 83*, 4978–4982.
Kolakofsky, D., Dewey, K. F., Herskey, J. W. B., & Thach, R. E. (1968) *Proc. Natl. Acad. Sci. U.S.A. 61*, 1066–1071.
Krøll, J. (1983) *Scand. J. Immunol., Suppl. No. 10*, 171–173.
la Cour, T. F. M., Nyborg, J., Thirup, S., & Clark, B. F. C. (1985) *EMBO J. 4*, 2385–2388.
Leberman, R., & Egner, U. (1984) *EMBO J. 3*, 339–341.
Maitra, U., Stringer, E. A., & Chaudhuri, A. (1982) *Annu. Rev. Biochem. 51*, 869–900.
March, P. E., & Inouye, M. (1985) *Proc. Natl. Acad. Sci. U.S.A. 82*, 7500–7504.
McCormick, F., Clark, B. F. C., la Cour, T. F. M., Kjeldgaard, M., Nørskov-Lauritsen, L., & Nyborg, J. (1985) *Science (Washington, D.C.) 230*, 78–82.
Möller, W., & Amons, R. (1985) *FEBS Lett. 186*, 1–7.
Morikawa, K., la Cour, T. F. M., Nyborg, J., Rasmussen, K. M., Miller, D. L., & Clark, B. F. C. (1978) *J. Mol. Biol. 125*, 325–338.
Peacock, S., Cenatiempo, Y., Robakis, N., Brot, N., & Weissbach, H. (1982) *Proc. Natl. Acad. Sci. U.S.A. 79*, 4609–4612.
Petersen, H. U. (1985) *Mat. Fys. Medd. K. Dan. Vidensk. Selsk. 41*, 291–335.
Plumbridge, J. A., Howe, J. G., Springer, M., Touati-Schwartz, D., Hershey, J. W. B., & Grunberg-Manago, M. (1982) *Proc. Natl. Acad. Sci. U.S.A. 79*, 5033–5037.
Plumbridge, J. A., Deville, F., Sacerdot, C., Petersen, H. U., Cenatiempo, Y., Cozzone, A., Grunberg-Manago, M., & Hershey, J. W. B. (1985) *EMBO J. 4*, 223–229.
Robakis, N., Meza-Basso, L., Brot, N., & Weissbach, H. (1981) *Proc. Natl. Acad. Sci. U.S.A. 78*, 4261–4264.
Robakis, N., Cenatiempo, Y., Meza-Basso, L., Brot, N., & Weissbach, H. (1983) *Methods Enzymol. 101*, 690–706.
Sacerdot, C., Dessen, P., Hershey, J. W. B., Plumbridge, J. A., & Grunberg-Manago, M. (1984) *Proc. Natl. Acad. Sci. U.S.A. 81*, 7787–7791.
Shiba, K., Ito, K., Nakamura, Y., Dondon, J., & Grunberg-Manago, M. (1986) *EMBO J. 5*, 3001–3006.
Travers, A. A., Debenham, P. G., & Pongs, O. (1980) *Biochemistry 19*, 1651–1656.
Weissbach, H., Robakis, N., Cenatiempo, Y., & Brot, N. (1984) *Biotechniques 2*, 16–22.
Wierenga, R. K., & Hol, W. G. J. (1983) *Nature (London) 302*, 842–844.

Solution Structure of the Trp Operator of *Escherichia coli* Determined by NMR†

Jean-Francois Lefèvre,‡ Andrew N. Lane,§ and Oleg Jardetzky*
Stanford Magnetic Resonance Laboratory, Stanford University, Stanford, California 94305-5055
Received November 18, 1986; Revised Manuscript Received March 9, 1987

ABSTRACT: We have assigned the majority of the nonexchangeable protons in the NMR spectrum of the 20 base-pair fragment of DNA corresponding to the Trp operator of *Escherichia coli*. The sequence (CGTACTAGTTAACTAGTACG) also contains a Pribnow box (underlined). Variation of the intrinsic spin–lattice relaxation rate constants of the H8's along the sequence indicates that the structure of the oligonucleotide is not regular. Splitting patterns of the H1′ resonances in the deoxyriboses, obtained from a two-dimensional *J*-resolved experiment, allowed the dominant pucker mode of each nucleotide to be determined. Intranucleotide NOEs from the sugar protons H1′, H2′, and H3′ to the base protons were used to determine the conformation of each nucleotide (puckers and glycosidic torsion angles). The relative orientations of nucleotide units (roll, propeller twist, helical twist angle, and pitch) were calculated by using internucleotide NOEs between protons of neighboring nucleotides in the sequence. All these parameters were determined for each step along the 20-mer. The structure belongs to the B family of conformations, but variations of the local geometry are observed from step to step. Some of the variations, such as the roll and the twist angles, can be predicted by the rules of Calladine and Dickerson [Calladine, C. R., & Dickerson, R. E. (1983) *J. Mol. Biol. 166*, 419–441]. The puckers of the deoxyriboses of purines are found mainly in conformations near C2′ endo, while those of the pyrimidines prefer C3′ endo and related conformations. Glycosidic torsion angles obtained for purines are larger than those of pyrimidines. Except for this last observation, the general properties of the operator DNA structure are comparable with those of crystal structures of B DNA of other sequences.

The control of gene expression by regulatory proteins that bind to specific sequences of DNA with affinities an order of magnitude greater than their affinity for bulk DNA must involve highly stereospecific interactions. Knowledge of the detailed structure of these specific sequences, such as the operator sequences binding repressors, is therefore important for the understanding of these interactions and the structural changes involved in the action of corepressors and inducers.

As part of an NMR study (Lane & Jardetzky, 1985a–c; Lefèvre et al., 1985a,b; Lane et al., 1986a,b; Lane, 1986) of the operator–repressor interaction in the Trp operator system

† This work was supported by NIH Grant RR00711 and NIGMS Grant GM33385. A.N.L. is grateful to EMBO for a long-term fellowship and J.F.L. to NATO and the Philippe Foundation for fellowships.
* Author to whom correspondence should be addressed.
‡ Present address: Institut de Biologie Moleculaire et Cellulaire, 67000 Strasbourg, France.
§ Present address: National Institute for Medical Research, The Ridgeway, Mill Hill, London NW7 1AA, U.K.

0006-2960/87/0426-5076$01.50/0

(Kelly & Yanofsky, 1985, and references therein), we have investigated the structure of the operator DNA. The sequence of the operator is (Gunsalus & Yanofsky, 1980)

CGTACTAGTTAACTAGTACG

The determination of the solution structure of DNA fragments relies heavily on the interpretation of nuclear Overhauser effect (NOE), since the magnitude of the effect depends on internuclear distances. Structures based on a direct estimate of the distances from NOE intensities observed in a 2D-FT (NOESY) experiment and refined by using a distance geometry algorithm (Clore et al., 1985) or restrained molecular dynamics (Clore et al., 1986) have been reported. Our analysis, however, shows that the direct method of estimating distances from NOE intensities is sufficiently inaccurate to yield inconsistent distances and incorrect structures. The key difficulty is found to lie in the existence of indirect pathways of magnetization transfer.

The correct analysis of NOE data involves the solution of the density matrix (Macura et al., 1981) which takes indirect magnetization transfer completely into account. Such an analysis, however, requires prior knowledge of the structure. The relaxation matrix contains the information on the internuclear distances. For structures of the size of an operator DNA fragment, and at the present state of computer technology, the iterative solution of the complete density matrix, varying the structure until agreement with experimental data is observed, is computationally prohibitive.

We have therefore developed a program for the analysis of NOE data that is based on the classical approximation in the form of generalized Bloch equations, which takes indirect pathways into account to first order:

$$dM_{zi}/dt = -\rho_i(M_{zi} - M_{z0i}) - \sum_{j \neq i} \sigma_{ij}(M_{zj} - M_{z0j}) \quad (1)$$

M_{zi} and M_{z0i} are the z components of the magnetization of the spin i at time t and at equilibrium, respectively. ρ_i is the longitudinal relaxation rate constant of the spin i. σ_{ij} is the cross-relaxation rate between nuclei i and j. NOE values are calculated by numerical integration of eq 1. The local structure is varied until agreement is found between the experimental and the calculated values of a related set of NOE. The advantage of this approach is that eq 1 can be solved numerically in a reasonable number of CPU hours of computer time. The principle of this approach has some similarity with the procedure recently described by Keepers and James (1984), Broido et al. (1985), Jamin et al. (1985), and Massefski and Bolton (1985) for nucleic acids and by Olejniczak et al. (1986) for peptides. In agreement with these authors, we have found that treating the complete spin system by solving eq 1 yields an internally consistent interpretation of the data. In addition, this approach allows us to detect subtle structural features obscured by a more approximate analysis of the data. Some general aspects of the method have been previously described (Jardetzky et al., 1986).

Materials and Methods

Operator DNA was purchased from P-L Biochemicals Limited and used without further purification. The purity and the duplex form of the oligonucleotide have been previously established (Lefevre et al., 1985a; Lane et al., 1986a). Two separate lots of DNA were purchased, one giving a solution of 1.5 mM in duplex, i.e., 3 mM in strands, and the second 5 mM in strands. The DNA was lyophilized from 99.7% D_2O and dissolved in 100% D_2O containing 10 mM sodium phosphate, 100 mM NaCl, pD* 8.5. The spectra of the two samples were indistinguishable and yielded the same results in a variety of spectroscopic tests.

Proton NMR spectra were recorded on a JEOL GX 500 spectrometer and a GE 500 spectrometer. For one-dimensional spectra, 16 384 data points were sampled over a spectral width of 5000 Hz. Prior to Fourier transformation, the spectra were apodized with an exponential function, adding 2 Hz to the line widths for relaxation experiments and 6 Hz for nuclear Overhauser effect experiments. Spectra were referenced to internal 2,2-dimethylsilapentane-5-sulfonic acid (DSS). NOESY spectra were recorded by using the standard pulse sequence (Jeener et al., 1979; Bax, 1982) with 2048 or 1024 points in the F2 dimension and 192 points in the F1 dimension, zero-filled to 1024 or 512 points as appropriate. Two hundred scans per slice were recorded, for a total acquisition time of about 35 h. Prior to Fourier transformation, the data matrix was multiplied by resolution enhancement functions, consisting of a trapezoidal window convoluted with a line-broadening exponential. The mixing times were 300 and 400 ms. COSY spectra were similarly recorded, with 2048 points in F2 and 192 points in F1, zero-filled to 1024 points. The final digital resolution was 4.4 Hz per point. The phase-sensitive NOESY spectrum was obtained by using the method of States et al. (1982), with 4096 points in F2 and 256 points in F1, zero-filled to 1024 points over a spectral width of 6000 Hz. The FIDs were multiplied by a double-exponential function (DM = 4) in both dimensions, equivalent to convolution difference. The mixing time was 200 ms and the temperature 25 °C.

The J-resolved 2D spectrum was acquired with the standard pulse sequence (Bax, 1982) at 35 °C to improve the resolution. Four thousand ninety-six points for a sweep width of 5000 Hz were used in F2, and 64 points zero-filled to 128 for a frequency range of 250 Hz were used in F1. Resolution enhancement in F2 and a line broadening of 1 Hz in F1 were applied during the processing. All 2D data are displayed as contour plots.

Spin–spin relaxation times (T_2) were obtained by using the Carr–Purcell–Meiboom–Gill method. Selective T_1 values were measured by using the pulse sequence $D1$–t–90x–Acq–$D3$. The decoupler was applied to the resonance of interest for a time $D1$. This was sufficiently short that no appreciable NOE builds up on other nearby protons, but was long enough that selectivity was maintained. A reasonable compromise was 25 ms. The power of the decoupler pulse was adjusted to saturate the resonance. t is a variable delay to allow relaxation to occur before observing the magnetization with a calibrated 90° pulse. The sum of the acquisition period and the postacquisition delay $D3$ was chosen to be $>5T_1$.

Driven, truncated NOEs (Wagner & Wüthrich, 1979) were also measured by using the pulse sequence for the selective T_1. In this instance, t is a fixed short delay to permit ringdown (0.5 ms), and $D1$ is variable. Again, the power of the decoupler pulse was adjusted to ensure saturation of the resonance [high-power limit; Bothner-By and Noggle (1979)], and the sum of the acquisition time and $D3$ was $>8T_1$. For the largest NOEs (>0.1), 500–1000 scans were recorded on and off resonance, whereas for the weak NOEs (<0.1), up to 3000 scans were recorded. For well-resolved resonances, the NOE was calculated by comparing the intensity of the difference peak with that in the off-resonance spectrum. For the poorly resolved resonances, the area of the difference peak was compared with that of a single proton. As least three values of $D1$ were used to define the NOE buildup curve. A total of about 100 experiments were then performed to achieve a usable data set.

Table I: Chemical Shifts of Nonexchangeable Protons of the Trp Operator DNA[a]

	chemical shift (ppm)								
base	H8	H6	H5 (Me)	H2	H1′	H2′	H2″	H3′	H4′
C1		7.64	5.87		5.77	1.99	2.42	4.70	4.08
G2	7.97				5.98	2.67	2.78	4.97	NA[b]
T3		7.26	(1.50)		5.72	2.10	2.45	4.90	NA
A4	8.29			7.30	6.20	2.74	2.85	5.03	4.41
C5		7.28	5.20		5.65	2.06	2.45	4.88	4.08/12
T6		7.30	(1.56)		5.73	1.92	2.45	4.84	NA
A7	8.16			7.05	6.03	2.69	2.87	5.03	4.15
G8	7.53				5.85	2.42	2.65	4.87	4.39
T9		7.15	(1.19)		5.95	1.93	2.44	4.87	NA
T10		7.32	(1.57)		5.66	1.97	2.33	4.62	NA
A11	8.23			6.82	5.90	2.69	2.86	5.06	4.19
A12	8.08			7.45	6.03	2.60	2.76	4.97	4.43
C13		7.17	5.08		5.70	2.02	2.43	4.86	4.08/12
T14		7.30	(1.52)		5.67	1.97	2.48	4.85	NA
A15	8.18			7.05	6.03	2.69	2.85	5.03	4.42
G16	7.56				5.81	2.40	2.68	4.87	4.15
T17		7.17	(1.28)		5.67	2.04	2.41	4.84	NA
A18	8.27			7.50	6.19	2.66	2.85	5.03	4.37
C19		7.28	5.34		5.65	1.83	2.27	4.60	NA
G20	7.87				6.13	2.33	2.58	4.67	4.18

[a] Assignments were made according to the text, at 25 °C. The assignments of the H2 resonances of adenine residues are from Lefèvre et al. (1985a). [b] NA = not assigned.

Results and Discussion

(1) Assignment of the Nonexchangeable Protons

The imino protons and the H2's of adenine residues were assigned by one-dimensional nuclear Overhauser enhancement (NOE) experiments as previously reported (Lefèvre et al., 1985a). The remaining base and sugar protons were assigned by using the now well-known method of sequential connectivities using two-dimensional spectroscopy (Hare et al., 1983; Clore & Gronenborn, 1983; Weiss et al., 1984; Scheek et al., 1984).

Figure 1 shows a ^{1}H NMR spectrum of the fragment, with assignments to general types of proton based on chemical shifts. Further general assignments can be made according to the following considerations. First, the only doublets that are expected to resonate to low field of the residual HDO (4.8 ppm) are from the 5 and 6 protons of cytosine. Second, the chemical shift of the H2″ protons of the deoxyribose moiety is always greater than that of the H2′ of the same sugar, and the H2′ of a ribose attached to a pyrimidine always resonates at higher field than the H2″ of a purine in B DNA (Hare et al., 1983; Scheek et al., 1984). The definite assignments were obtained by using a combination of 2D correlated spectroscopy (COSY) and 2D NOE spectroscopy (NOESY).

The so-called sequential assignment method relies on dipolar coupling between neighboring protons. There are two routes for following the coupling (Clore & Gronenborn, 1983; Hare et al., 1983; Weiss et al., 1984; Scheek et al., 1984). The first is to connect the H8/H6 of the bases to their own H1′, which interact also with the H6/H8 of the 3′ neighbor. Figure 2 shows the low-field region of a phase-sensitive NOESY spectrum, with H1′ to base proton connectivities drawn. The second route uses the dipolar coupling between the H8,H6 and the H2′ of its own sugar and between the H2″ of this sugar and the H6,8 of its neighbor in 3′. The H1′, H2′, and H2″ are scalar coupled one with the other, so they can be assigned by using a combination of COSY and NOESY. Usually both routes have to be used, though in many cases the two methods confirm one another. We were able to follow all of the connections via the first route and could therefore test it with the second. We were also able to obtain the same set of assignments on both samples of DNA, with agreement between the chemical shifts of ±0.02 ppm, which is within the experimental error.

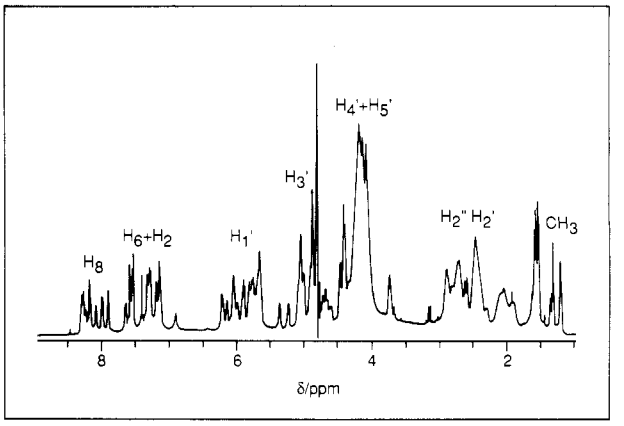

FIGURE 1: ^{1}H NMR spectrum of the Trp operator DNA at 500 MHz, in D_2O, 25 °C. The oligonucleotide is 3 mM in duplex, in 100 mM sodium phosphate, pD* 7.5. The spectrum is referenced to internal DSS. Assignments to proton types based on their chemical shifts are shown.

Table I is a compilation of the chemical shifts of the assigned nonexchangeable protons at 25 °C. Of 188 protons, we have assigned 128, the remainder being H5′, H5″, and some H4′. As expected, the chemical shifts of quasi-equivalent protons in the repeated sequence are very similar and in some instances are indistinguishable. The assignments were independently confirmed by one-dimensional NOE experiments used in the structure determination (see below).

(2) Gross Structural Features of the Trp Operator in Solution. Evidence for Irregularity of the Structure

We have previously shown that under the conditions of our experiments, the Trp operator fragment is double stranded in solution (Lefèvre et al., 1985a; Lane et al., 1986a). The melting temperature under these conditions is 55 °C, and the circular dichroism spectrum (not shown) is consistent with a right-handed B DNA conformation.

Irregularity in the Relaxation Rates. In a perfectly regular structure, all the sugar puckers, glycosidic torsion angles, and base-pair rolls and tilts would be identical. This would imply a certain uniformity of the observed NOE intensities and

Table II: Relaxation Times of H8 Protons of the Trp Operator[a]

	ρ_1 (s^{-1})				ρ_2 (s^{-1})		
proton/base	0 °C	10 °C	25 °C	40 °C	25 °C	35 °C	E_{app} (kcal/mol)
H8 G2	nd	nd	5.0	3.4	20	12.8	4.8
H8 A4	5.0	nd	4.2	3.1	19.6	14.9	3.8
H8 A7/15	8.0	5.9	4.2	2.3	22.7	14.1	4.5
H8 G8/16	nd	6.7	nd	1.9	nd	nd	nd
H8 A11	9.1	8.7	7.7	4.5	34.5	nd	3.2[b]
H8 A12	11.5	9.1	6.3	2.2	22.7	14.1	0.8[b]
H8 A18	5.0	nd	4.2	3.1	19.6	11.1	3.8
H8 G20	nd	5.6	3.8	2.5	15.2	11.2	4.2

[a] ρ_1 values were measured by using selective saturation recovery as described under Materials and Methods. ρ_2 values were obtained by using the Carr–Purcell–Meiboom–Gill method. The error of the relaxation rates is ±10% for the resolved residues, and ±20% for overlapping residues such as T9 H6. E_{app} is the apparent activation energy for the temperature dependence of ρ_1. nd = not determined. [b] Eyring plot is nonlinear; value of E_{app} for 0–25 °C.

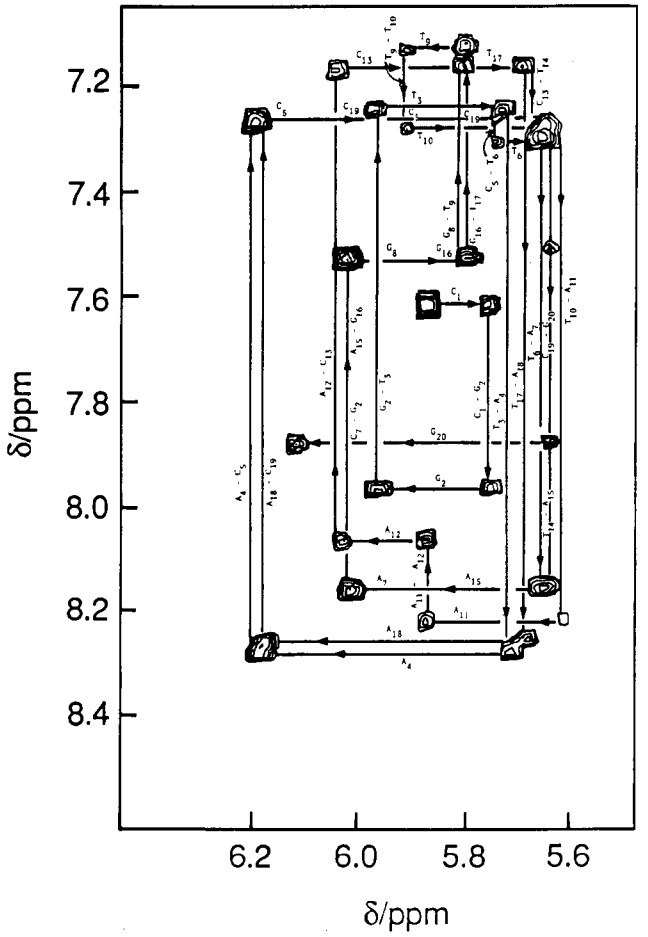

FIGURE 2: Phase-sensitive NOESY spectrum. Conditions were as in Figure 1. 4096 points were taken in F2 and 256, zero-filled to 1024 in F1, over a spectral width of 6000 Hz (digital resolution 5.9 Hz/point). The mixing time was 200 ms. The region shown includes the base, H1′ and H3′ protons. The lines show the sequential connectivities H1′ to base to H1′.

coupling patterns in the sugars. However, the NOE intensities of the interactions between the H8 and H1′, H2′, and H2″ are not identical (see Figure 2 and NOEs given in Table IV), implying the existence of sequence-dependent conformational variability.

In B DNA relaxation of the H8's of purines is dominated by the interaction with their own H2′ and the 5′ neighboring H2″. In a regular structure the intrinsic spin–lattice relaxation constant and the spin–spin relaxation rate constant would be essentially independent of the sequence. Calculations on regular B DNA indicate a variability due to the sequence of less than 10% in the relaxation times. The measured intrinsic spin–lattice and spin–spin relaxation rate constants for the H8's are given in Table II. Two points arise from these.

(1) Assuming standard geometry, the values at 25 °C of ρ_1 and ρ_2 should be about 7 and 17 s^{-1}, respectively [τ_R = 6.4 ns; Lane et al. (1986a)]. We attach no special significance to the absolute calculated values, though they are close to the observed values. More significant is that the relaxation rate constants vary by up to a factor of 2 along the sequence (for instance, between H8 of G20 and A11), which is clear evidence that the local structure (or dynamics) is sequence dependent. We have previously shown (Lane et al., 1986a,b) that the correlation time obtained from the cross-relaxation rate constant for the H5–H6 of cytosine residues and H6–methyl of thymine residues at different locations in the molecule accounts for the overall tumbling of the molecule. Further, internal motions of the base pairs are of insignificant amplitude on the nanosecond time scale. Therefore, it is likely that the observed variation of ρ_1 and ρ_2 with sequence reflects local, sequence-dependent, variations in conformation, rather than in dynamics.

(2) For a rigid body the relaxation rate constants should decrease as the temperature is raised, and the apparent activation energy should be about 4 kcal/mol (Lane et al., 1986a). Most of the protons do indeed have an activation energy of about 4–5 kcal/mol (see Table II). Those protons that do not yield an apparent activation energy close to 4–5 kcal/mol (i.e., the H8's of A11 and A12) probably experience local changes in conformation as the temperature is varied. Because of the r^{-6} dependence of the relaxation rate constants, the conformational changes could be quite small.

We have found a selective change with temperature in the relaxation parameters of the base protons on the TAA sequence of the Pribnow box (Lefèvre et al., 1985b), which explains the behavior of A11 and A12. We will give a detailed analysis of the temperature effects on these residues in a subsequent paper.

Irregularity of Spin Multiplicities in the Deoxyriboses. The dominant sugar pucker can be obtained from the coupling constants between the sugar protons (Davies, 1978). However, for a molecule of M_r 12 000, some of the line widths will be greater than the coupling constants, so the splitting cannot be observed. Fortunately, the H1's are relatively isolated and can be expected to have line widths in the range 2–3 Hz. Further, these protons are spread out in frequency, covering a range of 0.56 ppm or 288 Hz at 500 MHz (cf. Table I). The coupling of the H1's to the H2′ and H2″ permits a distinction to be made between puckers near C2′ endo and C3′ endo. The coupling of H1′ to two protons causes the peaks to be split into doublets or triplets, causing considerable overlap of the multiplets in one-dimensional spectra (see Figure 1). Because the widths of the H1′ resonances are inherently small compared with typical coupling constants (5–10 Hz), it is possible to resolve this region of the spectrum by two-dimensional *J*-re-

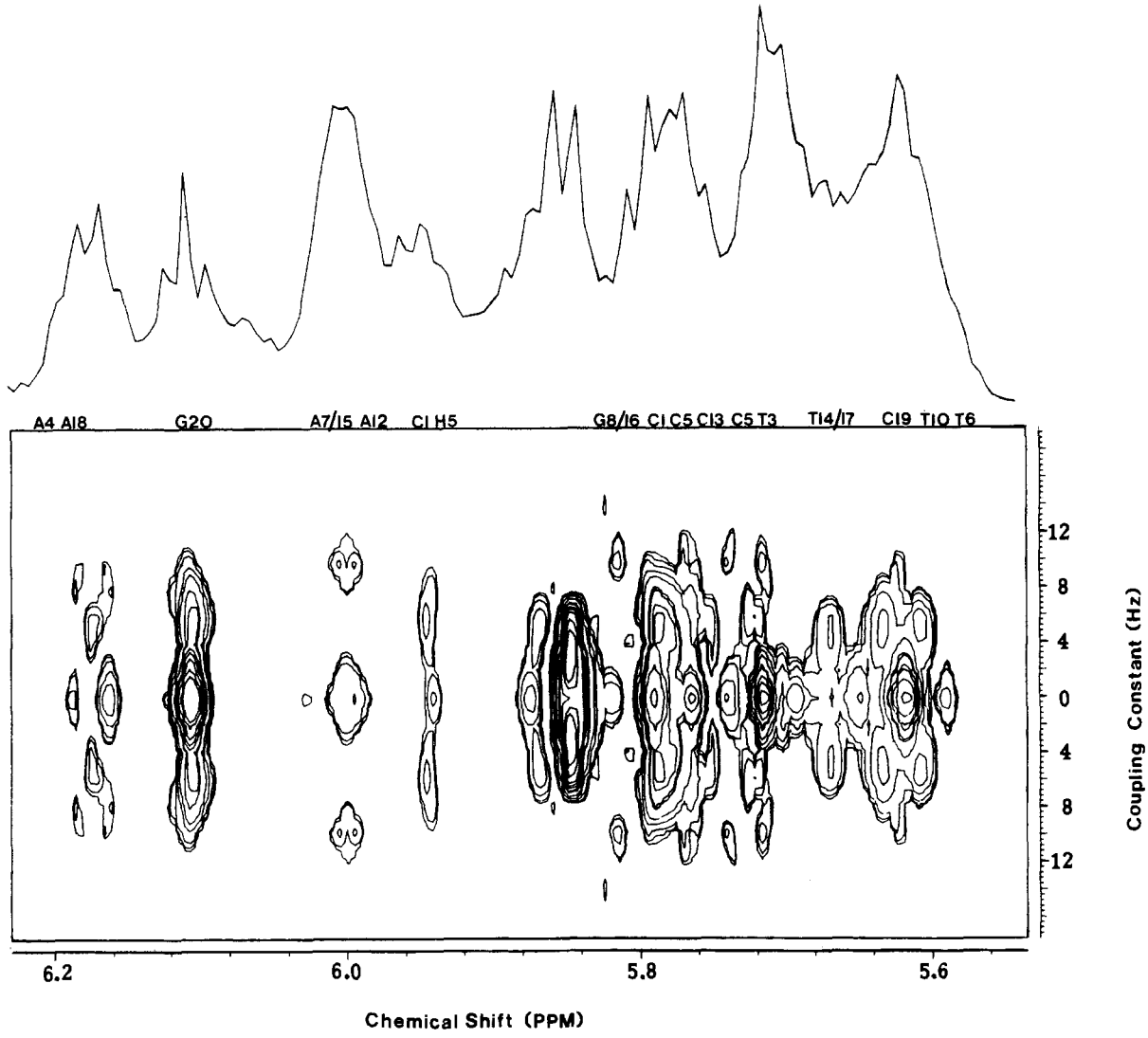

FIGURE 3: Two-dimensional *J*-resolved spectrum of the Trp operator DNA in D_2O. Only the H1′ region is shown. The oligonucleotide was 1.4 mM in duplex, in 100 mM sodium phosphate, pH 8.5, at 35 °C. 4096 points were taken in F2, giving a digital resolution of 2.44 Hz. In F1, 64 points zero-filled to 128 were used, for a digital resolution of 1.95 Hz. Resolution-enhancement functions similar to the one used for COSY (see Figure 2) were applied in F2, and a line broadening of 1 Hz in F1. Note that the δ values in this figure (sample at 35 °C) do not match the values given in Table I and Figure 1 (sample at 25 °C) due to the difference in sample temperature.

solved spectroscopy. In order to make the lines narrower, we recorded a *J*-resolved spectrum at 35 °C; the H1′ region is shown in Figure 3. When sufficient resolution enhancement is used in F2, approximately 20 multiplets can be seen, corresponding to the 20 H1′s present.

The coupling pattern of the H1′ to the H2′ and H2″ permits major pucker types to be distinguished. Doublets are expected for conformations in the north near 3′ endo, and triplets should be observed for conformations in the south (2′ endo, simulation not shown). Only the dominant pucker type can be determined from such experiments. It is not necessary to measure coupling constants accurately, as pseudorotation is likely to average the coupling constants, making a precise definition of the pseudorotation phase angle meaningless. Indeed, the multiplicity is characteristic of the dominant pucker present; one can only discriminate between near C2′-endo and near C3′-endo conformations.

The H1′s of the purine tend to resonate at lower fields than the H1′s of pyrimidines (Table I). At low field the multiplets appear mainly as triplets (Figure 3), whereas at higher fields the multiplets appear as doublets. The apparent multiplicities and the equivalent pucker type are given in Table III. The majority of the purines lie in the configuration range C1′ exo to C3′ exo, while the pyrimidines apparently occupy a much broader range of conformations from C3′ endo to O4′ exo. Such behavior has been noted before (Fratini et al., 1982).

In principle, the spin multiplicities of the H2′ and H2″ would give additional information on the puckers. Unfortunately, because the H2′ and H2″ resonances are broad (line widths >10 Hz), most of the splitting patterns for these atoms are not resolved.

(3) Structure Determination Using Nuclear Overhauser Enhancements

The nuclear Overhauser enhancement is widely used for structure determination because of its dependence on the inverse sixth power of interproton distances. For macromolecules, a common strategy is to estimate a large number of interproton distances and then reconstruct the molecule by using some form of distance geometry (Braun & Gō, 1985; Clore et al., 1985). For DNA one can reasonably assume a starting structure, e.g., right-handed B DNA, especially if there is independent evidence of the gross structure (see above). An alternative (Clore et al., 1986) is to use the distances obtained from NOEs as restraints in a restrained molecular dynamics calculation. The distances for the "refined" structure can then

Table III: Apparent Multiplicities and Sugar Patterns[a]

doublets for north (C3′ endo)		triplets for south (C2′ endo)	
Pu	Py	Pu	Py
(G2)			C1
	(C5)		T3
	T6	A4	
	(T9)	A7	
	T10	G8	
(A11)		A12	
	C13	A15	
	T14	G16	
	C19		T17
		A18	
		G20	
2[b]	7[b]	8[b]	3[b]

[a] The coupling patterns were obtained from the *J*-resolved spectrum at 35 °C (Figure 3). Parentheses indicate that the identification of the multiplets is uncertain. The north and south conformations are defined as

[b] Total.

be translated into conventional nucleic acid structural parameters.

As we will show below, however, a simple interpretation of an NOE in terms of precise distances can lead to internally inconsistent results. Structures derived by procedures that rely on them need to be verified by solving the Bloch equations before they can be accepted as correct.

Structural Parameters To Be Determined. It is common to report the structural parameters in DNA as torsion angles (Saenger, 1984). The glycosidic torsion angle, χ, and the pseudorotation phase angle, P, describe the structure of each nucleotide. The helical twist, θ_t, the base-pair roll, θ_R, the propeller twist, θ_p, and the base-pair tilt, t, give the orientation of the bases with respect to one another. Two other parameters describe the relative location of the helix axis and the vertical translation of each base pair. These are the helix displacement, D, and the local rise, h. We do not include, in this analysis, the torsion angles in which phosphates are involved, because it is known that these angles are subject to more extensive motional averaging than the bases (Hogan & Jardetzky, 1979, 1980; Keepers et al., 1982). We therefore did not collect any ^{31}P NMR data on that part of the molecule for purposes of structure determination.

The glycosidic torsion angle is defined by the atoms C8, N9, C1′, and O4′ for purines and C2, N1, C1′, and O4′ for pyrimidines.

Puckering in the deoxyribose ring was modeled by using the pseudorotation formalism of Altona and Sundaralingam (1972) with the value of ν_{max} fixed at 38.6° (Saenger, 1984) and the phase angle P as the variable. A 10% variation in ν_{max} corresponds to an error of less than 10° in P, which is smaller than the experimental error in P. The phase angle is related to the five ring torsion angles ν_j (Altona & Sundaralingam, 1972)

$$\nu_j = \nu_{max} \cos (P + j\,144) \qquad (2)$$

with $j = 0$ for the C2′–C3′ bond, 1 for the C3′–C4′ bond, 2 for the C4′–O4′ bond, and so on, until $j = 4$. The phase angle corresponds to sugar puckers as follows: C3′ endo ($P = 18$), C4′ exo ($P = 54$), O4′ exo ($P = 90$), C1′ exo ($P = 126$), C2′ endo ($P = 162$), and C3′ exo ($P = 198$).

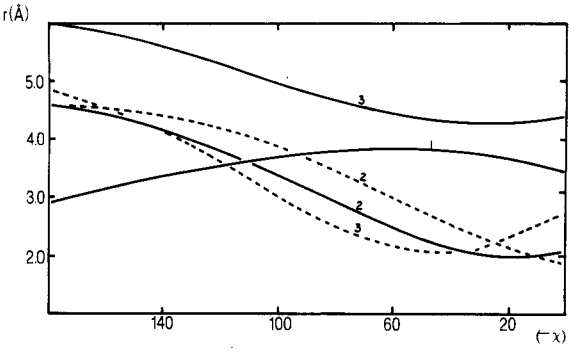

FIGURE 4: Dependence of distances on the glycosidic torsion angle in purines. Continuous lines are for C2′ endo and the dotted lines are for C3′ endo. Distance between (1) H1′ and H8, (2) H2′ and H8, and (3) H3′ and H8.

The helical twist (θ_t) is defined as a rotation about the local helix axis, the base-pair roll (θ_R) as a rotation about an axis perpendicular to the pseudodyad, passing through C8 and C6, and the base-pair tilt (t) as a rotation about the pseudodyad axis.

From the point of view of the NMR experiments, it was convenient to define apparent roll angles of individual bases, which is the sum of the base-pair roll and the propeller twist (θ_p). The apparent roll angles R_1 and R_2 of the two bases in a base pair are then related to the base-pair roll and propeller twist by

$$\theta_R = (R_1 - R_2)/2 \qquad \theta_p = R_1 + R_2 \qquad (3)$$

$R_{1,2}$ is positive when the base, viewed from its C8,6, rotates clockwise about the C8–C6 axis of the base pair (roll axis). θ_R is defined here as the angle between the best mean plane through the base pair and a plane perpendicular to the helix axis. This angle measures the degree of rolling of an individual base pair, and its sign depends on the strand from which the base-pair plane is observed. However, the roll angle is most commonly defined as a measure of the extent to which the best mean planes through two successive base pairs open toward the minor groove (Fratini et al., 1982). This inter base pair roll angle (θ_r) is positive when the base pairs open toward the minor groove and is related to θ_R by

$$\theta_r = \theta_R(5') - \theta_R(3') \qquad (4)$$

where $\theta_R(5')$ and $\theta_R(3')$ are the roll angles, defined with respect to the same strand, of the base pairs in 5′ and 3′, respectively.

For purposes of distance calculation and graphic display, the standard heavy-atom coordinates of the nucleotides were initially taken from Arnott and Hukins (1972) and transformed into Cartesian coordinates. Translation and rotation due to local helix parameters were then applied to the base. The sugar skeleton and all protons were added by constructing scalar and vector products of known and unknown interatomic vectors using standard bond lengths and bond angles and torsion angles defined above. This gave sets of simultaneous equations for the coordinates, which were obtained by matrix inversion. The coordinates were checked by calculating C–C and C–H bond lengths, which deviated from the standard values by less than 1%.

Set of NOEs Used To Determine the Structural Parameters. The following NOEs between protons can be used to determine the structural parameters defined above.

(1) Intranucleotide NOEs are found between sugar protons (H1′, H2′, H2″, and H3′) and base protons (H8 or H6). Figure 4 shows the variation of the distances between the H1′, H2′, and H3′ and the purine H8 as a function of the glycosidic

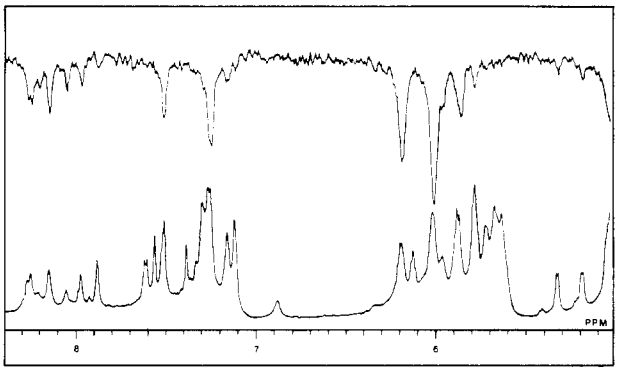

FIGURE 5: Trp operator DNA reference spectrum (lower) and NOE difference spectrum (upper) obtained by irradiating at 2.85 ppm (irradiation time: 100 ms). The observed NOEs are intra H2″–H8 NOEs for A4 (8.29 ppm), A7/15 (8.18 ppm), and A18 (8.27 ppm); inter H2″–H8 NOE for G8/16 (7.53 ppm), H2″–H6,5 NOEs for C5 (7.28 and 5.20 ppm) and C19 (7.28 and 5.34 ppm); and H2″–H1′ NOE for the deoxyribose of A4 and A18 (6.20 ppm).

torsion angle (χ) for two extreme puckers (2′ endo and 3′ endo). Similar curves were obtained for distances between pyrimidine sugar and base protons. The distance from the H1′ to the H8,6 is independent of the sugar pucker, so in principle could be used directly to determine the glycosidic torsion angle in the normal range observed for B DNA ($\chi \approx -40$ to $-60°$). On the other hand, both H2′–H8 and H3′–H8 distances are strongly dependent on the glycosidic torsion angle and on the sugar pucker. Unfortunately, the H3′–H8 distance is large in the C2′-endo conformation, implying weak NOEs. Nevertheless, one might hope to obtain initial estimates of the structural parameters from distances derived from NOEs.

(2) Internucleotide NOEs are observable between sugar protons (H1′ and H2″) and protons of the 3′ base (H8 or H6), between imino protons of neighboring bases, and between H6 or H8 of neighboring bases. When a pyrimidine step is involved, the H5 and the methyl protons can also be used. For methyl groups of thymines, an equivalent distance r_{eq} is calculated by using (Olejniczak et al., 1984)

$$1/r_{eq}^6 = (1/3)\sum_{i=1}^{3} 1/r_i^6 \qquad (5)$$

Theoretically, one has to determine 10 parameters per base pair, except for one end base pair for which helical twist and local rise are meaningless. Then for an oligonucleotide n base pairs long, the number of required distances is $10n - 2$. For the Trp operator oligonucleotide, this number is to be divided by two because of the palindromic symmetry. This sets the requirement to 99 measurable NOEs.

We therefore measured as many NOEs as possible at several different irradiation times (mainly 100, 200, and 300 ms). Figure 5 shows an NOE difference spectrum and the associated off-resonance spectrum for irradiation at a H2″ position. Similar difference spectra were obtained for at least three different irradiation times for each of the assigned lines. This provides us a total of 153 intranucleotide NOEs (51 different NOEs at three different times) and 153 internucleotide NOEs (51 different NOEs at three different times). Table IV gives the NOE data obtained at one irradiation time.

Analysis of NOEs in Terms of Distances. In the analysis of NOE data it is common practice to calculate an *apparent* cross-relaxation rate (σ_a = NOE/t) from the NOE value obtained at a time t. When the transfer of magnetization operates by the direct pathway, namely, when the protons are close together ($R \approx 2$–3 Å), the NOE buildup curve is essentially linear for short values of the irradiation time and σ_a asymptotically approaches the true σ value. In these cases, one time point is sufficient, and the distance can be calculated from the relation

$$\sigma = K\tau_c/r^6 \qquad (6)$$

provided the correlation time τ_c is known.

It is obvious, however, referring back to eq 1, that the use of eq 6 necessarily implies a two-spin approximation and that the calculated distances will be in error if indirect magnetization transfer plays a significant role. We therefore found it desirable to check the shape of the curve by using several irradiation times.

To estimate a distance from an NOE, we have initially used the approach recently described by Clore et al. (1985)

$$\mathrm{NOE}(t)/\mathrm{NOE}_c(t) = (r_c/r)^6\tau/\tau_c \qquad (7)$$

where NOE(t) is the value of the NOE at an irradiation time t, $\mathrm{NOE}_c(t)$ is the NOE for a calibration distance r_c, in this instance the H5 to H6 of cytosine (R = 2.47 Å), and τ and τ_c are the relevant correlation times. According to Clore et al. (1985), this calculation yields distances accurate to ±0.15 Å.

However, as it can be seen in Table IV, when we used distances directly derived from the NOEs in eq 7, we obtained conflicting results for the glycosidic torsion angle and the sugar pucker. For example, the distance from H1′ to H8 implies a value of χ in the range −120 to −160°. The H3′–H8 distance then requires that the sugar pucker be near C3′ endo. On the other hand, the distance for H2′–H8 requires a value of χ in the range −20 to −40° for C3′ endo and −40 to −60° for C2′ endo. The calculated distances are therefore incompatible. The first set of calculated distances would suggest a conformation of the A type, whereas the second set suggests a B type, which is more consistent with the circular dichroism spectrum and the overall pattern of NOEs in the NOESY spectrum.

Indirect magnetization transfer is an important source of error in the direct calculation of distances from eq 7 in a multispin system. It can increase the observed NOE and therefore decrease the apparent distance. If the observed NOE is twice as large as expected, the apparent distance will be 12% smaller. For H1′–H8 this amounts to about 0.5 Å and would account for the high-value χ estimated. On the other hand, large values of ρ_1 cause the NOE to build up rapidly, so that the linear approximation is valid only at very short times; the σ calculated from the observed NOE is underestimated by the linear approximation, thereby producing an increase in the apparent distance.

The problem of measuring NOEs in the particular multispin system represented by nucleic acids is illustrated in Table V. This table gives the "true" and the "apparent" distances. The former were deduced from the coordinates of the protons and used to simulate the time course of magnetization transfer, giving the NOE values at different mixing times (for this calculation a correlation time of 6 ns, corresponding roughly to a 20 base pair oligonucleotide at 25 °C, was taken). The latter were estimated from these calculated NOEs at two different mixing times (100 and 200 ms) by using eq 7. It is noteworthy that the apparent distances given in Table V are mutually inconsistent. Both cases described above can be observed.

(1) For distances larger than 3 Å the errors in the apparent distances are seen to be large. This is mainly true for H1′–H8,6 or H3′–H8,6 NOEs, from which the calculated distances are underestimated.

(2) For distances between 2 and 2.5 Å the calculated distances can be larger than the true distances. For instance, the

Table IV

(A) Intranucleotide NOEs[a]

base	protons	time (ms)	NOE	r(D)	χ(D)	r(N)	base	protons	time (ms)	NOE	r(D)	χ(D)	r(N)
C1	H1′–H6	250	0.09	3.17	−150	3.64	T10	H1′–H6	200	0.10	3.00	−168	3.69
	H2′–H6	100	0.13	2.56	−45, −70	1.80		H1′–CH_3	250	0.01	4.57	nd	6.23
	H2″–H6	200	0.07	3.18	nd	3.09		H2′H6	100	0.21	2.36	−37, −60	1.89
	H3′–H6	300	0.02	4.20	−50, −150	4.11	A11	H1′–H8	200	0.06	3.27	−150	3.79
G2	H1′–H8	200	0.06	3.27	−145	3.76		H2′–H8	100	0.23	2.33	−30, −52	2.22
	H2′–H8	100	0.29	2.24	−26, −47	2.15		H2″–H8	100	0.14	2.53	nd	3.62
	H2″–H8	100	0.08	2.77	nd	3.80		H3′–H8	200	0.05	3.37	nv, −115	4.21
	H3′–H8	200	0.07	3.18	nv, −110	3.03	A12	H1′–H8	200	0.07	3.18	−152	3.77
T3	H1′–H6	200	0.12	2.91	−168	3.68		H2′–H8	100	0.22	2.34	−31, −53	2.14
	H1′–CH_3	250	0.025	3.92	nd	6.22		H3′–H8	200	0.12	2.91	nv, −100	4.19
A4	H1′–H8	200	0.052	3.35	−139	3.79	C13	H2″–H6	50	0.13	2.28	nd	3.53
	H2′–H8	100	0.24	2.31	−30, −52	2.22		H2′–H5	100	0.02	3.49	nd	4.16
	H2″–H8	100	0.12	2.50	nd	3.62	T17	H1′–H6	200	0.04	3.49	−120	3.71
	H3′–H8	200	0.06	3.27	nv, −115	4.34		H2′–H6	100	0.24	2.31	−35, −60	2.10
C5	H2′–H5	200	0.06	3.27	nd	4.42		H3′–H8	200	0.08	3.11	nv, −110	2.66
T6/T14	H1′–H6	200	0.09	3.05	−159	3.71	A18	H1′–H8	200	0.03	3.67	−100	3.79
A7/A15	H1′–H8	200	0.04	3.49	−130	3.80		H2′–H8	100	0.24	2.31	−30, −52	2.22
	H2′–H8	100	0.18	2.42	−35, −58	2.31		H2″–H8	100	0.11	2.63	nd	3.62
	H2″–H8	100	0.10	2.67	nd	3.72		H3′–H8	200	0.06	3.27	nv, −115	4.21
	H3′–H8	200	0.09	3.05	nv, −105	4.37	C19	H2′–H5	100	0.02	3.49	nd	4.22
G8/G16	H1′–H8	250	0.06	3.39	−135	3.79		H3′–H5	200	0.08	3.11	nd	5.12
	H2′–H8	100	0.18	2.42	−35, −58	2.31	G20	H1′–H8	200	0.05	3.37	−135	3.79
	H3′–H8	200	0.09	3.05	nv, −105	3.24		H2′–H8	100	0.22	2.34	−31, −53	2.25
T9	H1′–H6	200	0.11	2.95	−168	3.69		H3′–H8	200	0.03	3.67	nv, −130	4.35
	H2′–H6	100	0.20	2.38	−53, −78	2.26							
	H2″–H6	200	0.12	2.91	nd	3.73							
	H3′–H6	200	0.16	2.77	nv, −100	1.96							

(B) Internucleotide NOEs[b]

obsd protons	irradiated protons	time (ms)	NOE	r(D)	r(N)	obsd protons	irradiated protons	time (ms)	NOE	r(D)	r(N)
G2-H8	C1-H1′	200	0.04	3.49	3.39	A11-H8	T10-H1′	200	0.08	3.11	3.44
	C1-H2′	200	0.07	3.18	4.47		T10-H2″	100	0.18	2.42	2.25
	C1-H2″	100	0.11	2.63	2.93		T10-H6	200	0.05	3.37	4.69
	T3-H6	200	0.02	3.92	5.22	A11–H2	T9-NH[f]	200	0.10	3.00	3.91
	T3-CH_3	100	0.05	3.00	4.97	A12-H8	A11-H1′	200	0.07	3.18	3.32
T3-H6	62-H1′	200	0.14	2.84	2.77		A11-H2″	100	0.12	2.59	2.47
T3-CH_3	G2-H1′	250	0.035	3.71	4.09		A11-H8	200	0.04	3.49	5.50
A4-H8	T3-H1′	200	0.04	3.49	3.54		C13-H6	200	0.05	3.37	5.25
	T3-H2′	200	0.06	3.27	3.13	A12-H2	A11-H2	200	0.16	2.77	4.21
	T3-H2″	100	0.07	2.84	2.83		G8-NH[f]	200	0.03	3.67	4.64
	T3-CH_3	100	0.07	2.84	6.13	C13-H6	A12-H1′	200	0.10	3.00	3.34
C5-H5	A4-H1′	200	0.05	3.37	4.22		A12-H2″	100	0.18	2.42	2.27
	A4-H2″	100	0.13	2.56	2.70	T17-H6	G16-H1′	200	0.14	2.84	3.47
T6-H6[c]	C5-H1′	200	0.07	3.18	3.00		G16-H2″	100	0.22	2.34	2.28
A7-H8[d]	T6-H1′	200	0.05	3.37	3.84	T17-CH3	G16-H1′	250	0.039	3.64	4.66
	T6-H2′	100	0.09	2.72	2.75	A18-H8	T17-H1′	200	0.03	3.67	3.78
	T6-H2″	100	0.08	2.77	2.86		T17-H2″	100	0.09	2.72	2.83
	T6-H6	200	0.04	3.49	4.24		T17-H6	200	0.03	3.67	4.46
G8-H8[e]	A7-H1′	250	0.10	3.11	3.34		C19-H6	200	0.03	3.67	5.11
	A7-H2″	100	0.18	2.42	2.19	C19-H5	A18-H1′	200	0.03	3.67	4.48
	T9-CH_3	100	0.04	3.11	2.80		A18-H2′	100	0.04	3.11	3.34
T9-H6	G8-H1′	250	0.19	2.80	3.35		A18-H2″	100	0.10	2.67	2.96
	G8-H2″	100	0.19	2.40	2.17	G20-H8	C19-H1′	200	0.06	3.27	3.18
T9-NH	G8-NH	200	0.05	3.37	3.95		C19-H2″	100	0.05	3.00	2.82
T10-H6	T9-H1′	200	0.19	2.70	2.43		C19-H6	200	0.04	3.49	5.05
T10-NH	T9-NH	200	0.07	3.18	3.40						

[a] The NOE at only one of the three used irradiation times is tabulated (third column). Temperature 25 °C. Correlation time 6.4 ns. r(D) and r(N) are the distance (in Å) between the irradiated and the observed protons, directly calculated according to eq 7 and deduced from the structural parameters given in Table VIII, respectively. χ(D) is, in degrees, the glycosidic torsion angle deduced from r(D). When two values are given, they correspond to the calculation in C3′ endo and in C2′ endo, respectively. The final values of χ can be found in Table VIII. Distances involving CH_3 groups are calculated according to (9). nd: not determined. nv: no value of χ found for the pucker. [b] At one of the three used irradiation times (third column). Temperature 25 °C. Correlation time 6.4 ns. All measurements were performed in D_2O except for NOEs involving imino protons, which were obtained in 85% H_2O, 15% D_2O. [c] Same NOE data for H6-T14. [d] Same NOE data for H8-A15. [e] Same NOE data for H8-G16. [f] On the opposite strand.

calculated H2′–H8 of adenosine compares quite well with the true distance, while H2′–H6 of cytosine is overestimated. This difference in the results is due to the higher relaxation rate of H6 compared with that of H8. However, it should be noted that the errors induced by the relaxation of the observed proton are smaller than the errors due to indirect magnetization transfer. The same type of results have been obtained by Olejniczak et al. (1984) in the analysis of simulated and experimental NOEs in lysozyme.

There are two solutions to the problem of spin diffusion. The first, favored by Wüthrich and co-workers (Chazin et al., 1986), is to use a very short mixing time such that spin diffusion becomes negligible. However, for nucleic acids, at least, many of the structurally useful NOEs become unobservable

Table V: Apparent Distances from NOEs in Standard B-DNA[a]

irradiated spin	obsd spin	r^{app} (Å) at 100 ms	r^{app} (Å) at 200 ms	r_{true} (Å)
AH1′	AH8	3.30	3.08	3.77
AH1′	AH2′	2.70	2.68	2.96
AH1′	AH2″	2.45	2.52	2.26
AH1′	CH6	2.90	2.87	3.04
AH1′	CH5	3.32	3.11	3.89
AH2′	AH8	2.15	2.17	2.13
AH2′	AH3′	2.32	2.30	2.36
AH3′	AH8	3.20	3.00	4.31
AH2″	AH8	2.53	2.39	3.50
AH2″	AH1′	2.27	2.25	2.26
AH2″	CH6	2.21	2.27	2.08
AH2″	CH5	2.45	2.39	2.51
CH6	CH1′	3.11	2.84	3.71
CH6	CH2′	2.15	2.22	1.96
CH6	CH3′	2.96	2.74	4.12
CH6	AH8	3.46	3.05	5.06
CH6	AH1′	2.77	2.63	3.04
CH5	AH8	3.37	3.17	3.65
CH5	AH1′	3.32	3.11	3.89
CH5	AH2′	2.89	2.83	3.12
CH5	AH2″	2.65	2.67	2.51

[a] NOE buildup curves were generated as described in Materials and Methods for a correlation time corresponding to 20 base pairs (6 ns). The dinucleotide has the sequence AC. The structural parameters are $\chi = -40°$, $P = 162°$, $h = 3.4$ Å, $\theta_t = 36°$, $\theta_r = 0°$, tilt = 0°. Apparent distances were calculated according to eq 7 by using the NOE from the H6 to the H5 of the cytosine residue ($r = 2.47$ Å). The irradiation times were 100 and 200 ms. For times shorter than 100 ms, many of the NOEs fall below 1%, which is taken as the lower limit of detectability. r_{true} is the actual input distance.

(e.g., H1′ and H3′ to H8,6) at very short mixing times (<50 ms). Without these NOEs, there is insufficient information available to determine the structure of the molecule uniquely. As soon as these NOEs become observable with an adequate signal-to-noise ratio, they are substantially contaminated by spin diffusion, as is shown by the data in Table V. This is simply an unavoidable consequence of the geometry of nucleic acids.

The second solution is to specifically take into account spin diffusion and use the additional information that is obtainable. This solution was taken in the work reported here. As a consequence of spin diffusion, the direct method of analysis of NOE data, using eq 6 and 7, is apt to produce incorrect distances. These errors can result in quite erroneous conclusions concerning the basic features of the DNA conformation.

NOE Analysis Taking into Account Indirect Magnetization Transfer. The time dependence of the z component of the magnetization after a perturbation is described by the generalized Bloch equations. The quantitative analysis of NOEs, accounting for the effects inherent in multispin systems and described above, can be performed by integrating the complete set of Bloch equations. This has been already suggested by us (Jardetzky et al., 1986) and others (Massefski & Bolton, 1985) and, for 2D NOEs, by Keepers and James (1984), Broido et al. (1985), and Olejniczak et al. (1986). The dependence of the rate constants in eq 1 on the internuclear distances and spectral density functions has been discussed in detail by Lane et al. (1986a).

Integration of the Bloch equations for irradiation of spin k (i.e., M_k is set to zero for a time t) yields the time courses of the magnetization of every spin that has significant dipolar coupling to the irradiated spin. NOE time courses corresponding to the driven truncated NOE experiment (Wagner & Wüthrich, 1979) in the high-power limit (Bothner-By & Noggle, 1979) were calculated by numerical integration of equations using Euler's method. The step size was automatically adjusted to $^1/_{40}\, r_{max}$, where r_{max} is the largest spin–lattice relaxation rate constant of the spin system. Calculations of exact time courses using the analytical expression for two or three spins (Wagner & Wüthrich, 1979) showed that this step size gives sufficiently accurate values of the NOE over the desired time course.

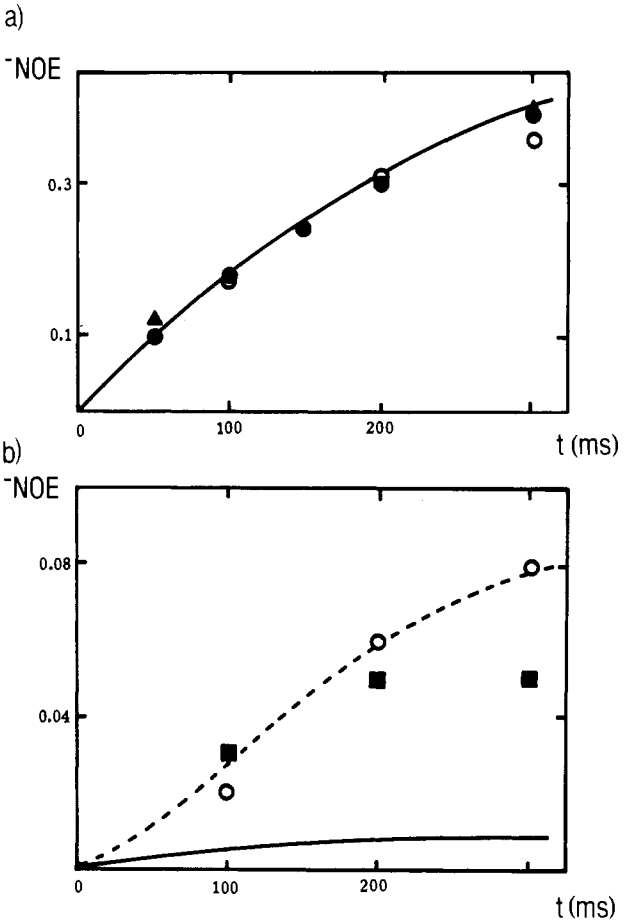

FIGURE 6: NOE buildup curve for the NOE. Same conditions as in Figures 1 and 5. NOE are observed (a) on H8 protons of A4 (▲), A11 (●), and A18 (○) by irradiating the H2′ protons of their own deoxyribose. The line corresponds to the function $0.5(1 - \exp(-4.5t))$. NOE are also observed (b) on H8 protons of A4 (○) and G20 (■) by irradiating the H3′ protons of their own deoxyribose. The dotted line is a fit to the NOE buildup curve for A4 from a complete spin system and represents the apparent buildup curve. The unbroken line corresponds to the direct NOE buildup curve, from the cross-relaxation rate constants between H3′ and H8 only, for a standard B structure.

We have systematically calculated the NOE time courses for nucleotides in a range of conformations. Typical results are shown in Figures 6 (time course for H1′–H8 intranucleotide NOR) and 7 (intranucleotide NOE as a function of pucker and glycosidic torsion angle). It is clear that ignoring indirect pathways of magnetization transfer can lead to very large errors in the estimation of σ (Figure 6) and consequently of the glycosidic torsion and pseudorotation phase angles (Figure 7). The curves in Figure 7, and similar curves for other parameters, can be used to obtain initial estimates of the torsion angles that can then be refined by a nonlinear least-squares program.

Incidentally, the curves in Figure 7 demonstrate that the intranucleotide NOEs are very sensitive to the value of χ in the range expected for B DNA (around −40°), but much less sensitive for A DNA ($\chi \approx -100°$). Also, the H3′ to H8 NOE is the most sensitive to the sugar pucker. However, we note that in the south conformation ($98° < P < 196°$) none of the NOEs are sensitive to the actual value of P, whereas in the

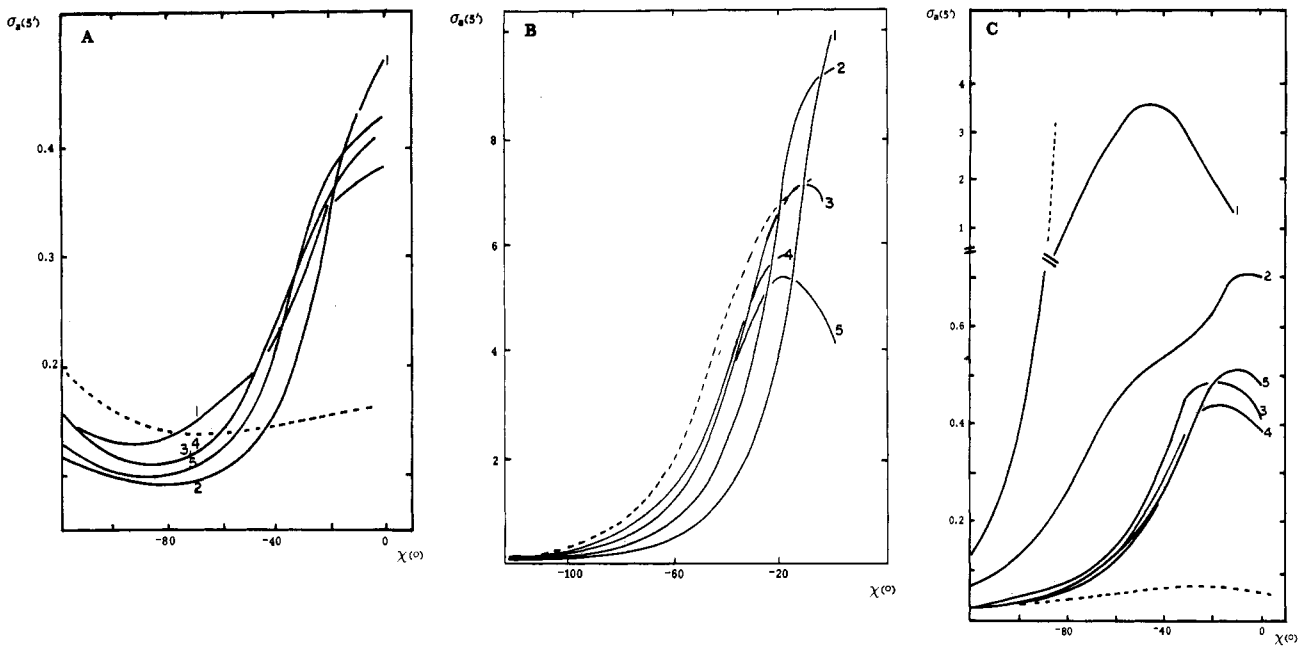

FIGURE 7: Dependence of the apparent cross-relaxation rate constant on glycosidic torsion angles and sugar pucker. Cross-relaxation rate constants (σ_a) were evaluated at 200 ms for H1′ and H3′ to H8 and at 100 ms for H2′ to H8. Continuous curves represent calculations including all protons in the nucleotide unit, and the dotted line for the corresponding two-spin system only (P = 162°): (1) P = 18; (2) P = 54; (3) P = 98/192; (4) P = 126; (5) P = 162. A: H1′–H8. B: H2′–H8. C: H3′–H8.

north conformation (−90° < P < 90°) the sensitivity is at its maximum.

Effects of Internal Motions. The correlation times of the cytosine H5–H6 and thymine CH_3–H6 vectors are all identical in the Trp operator and also are equal to the effective tumbling time of the molecule (Lane et al., 1986a). This implies that large-amplitude motions of the bases are not important in this fragment of DNA. On the other hand, pseudorotation in the deoxyribose is expected to be fast, affecting the correlation times of vectors connecting protons within a sugar (Röder et al., 1975). In deoxyribose the distance between H1′ and H2″ is almost insensitive to the pucker (r = 2.25 ± 0.03 Å), so the cross-relaxation rate constant for these protons can be used to calculate the correlation time of the pseudorotation in the DNA.

We have measured the NOE between H2″ and H1′ of A4 and A18 at different temperatures. A plot of the cross-relaxation rate constant (σ) against the viscosity/absolute temperature [Perrin plot, Lane et al. (1986a)] was linear (data not shown). Assuming M_r = 12 000, partial specific volume $\bar{v} + h$ = 1.1 mL/g^{-1} (Cantor & Schimmel, 1980), friction coefficient F = 1.1 (Lane et al., 1986a), and r = 2.25 Å, the slope of the Perrin plot gives $a_1 \approx 0.6$. This value of a_1 corresponds to an angle (taken for the component of the motion on the helix axis) of about 23°. This is very similar to the value esimated for the T and A sugars in $dA_{20}dT_{20}$ (Lane et al., 1986b). It is also possible to estimate this angle from the largest variation of the coordinate of H2″ along the helix axis when the deoxyribose explores all conformations. For a glycosidic torsion angle of −45°, the calculated value of this angle is 21°. It compares very well with the value deduced from the experimental data.

Examination of a molecular model of a nucleotide shows that the motion of the H1′ with respect to H8,6 is negligible when the pucker of the deoxyribose is changed. On the other hand, given the χ angles typical of B DNA, H3′ is displaced almost parallel to the base plane, so that the component along the helix axis of the motions of these protons is rather small if not zero. Therefore, the pseudorotation should not have a significant effect on the *direct* NOEs between these protons and the base-proton H8,6 due to decreases in the correlation time. However, for the glycosidic torsion angles adopted by the nucleotides, the observed NOEs from H1′ to H3′ to H8,6 are not only direct but have a significant contribution from the alternative pathways via H2′ and H2″. The analysis developed above shows that the motion of H2″ reduces the effective correlation time of the H1′–H2″ vector by ≤40%. This represents an upper limit to the effect on the other NOEs. However, the decrease in the effective correlation time is counterbalanced by the change in internuclear distance during the motion. Because the probable maximum effect of internal motion on the structurally useful NOEs is smaller than the experimental error, we have chosen to ignore it in the present analysis.

Pseudorotation will also affect the coupling constants in the sugar moieties. Simulations (not shown) indicate that mixing 30% C2′ endo with 70% C3′ endo produces a multiplicity for the H1′ similar to that of C2′ endo, whereas a 50:50 or a 30:70 mixture of C3′ endo–C2′ endo produces a triplet pattern similar to that of C3′ exo. Hence, the observation of a doublet for H1′ would imply the presence of C3′ endo with at most a small fraction of south conformations, whereas a triplet would be consistent with C3′ exo or a mixture of C2′ endo and C3′ endo.

Structure Refinement. It is important to note that the structural information obtainable by NMR reflects *local* structural features. A map of all local conformations will yield the complete structure of an oligonucleotide. However, protons from one local structural unit can be in dipolar interaction with protons of the neighboring unit. In this case, the spin–lattice relaxation rate, which is needed to solve the Bloch equations for the local spin system, cannot be calculated a priori. The difficulty can be overcome by using the *experimental* value of the relaxation rate constants (some of these data are given in Table II) when solving eq 1.

It is therefore justified to derive the structure of an oligonucleotide by a two-step procedure. First, the conformation of each nucleotide can be determined individually by using

intranucleotide NOEs. Then the oligonucleotide molecule can be constructed by the assembly of overlapping dinucleotide units. In each dinucleotide the orientation of the 5′ nucleotide with respect to the 3′ one is determined by using internucleotide NOEs, which depend on the roll of the base, the helical twist, and the local rise between the bases. In determining these parameters the previously determined conformation of each nucleotide is unchanged. It should be noted that the twist angle and the local pitch are shared by the two dinucleotides on opposite strands.

Initial values of the structural parameters as determined from the plots of the NOE as a function of the parameters (see Figure 7) were refined by fitting a set of simulated NOEs to those observed. The best fit was found by minimizing residuals

$$\Delta^2 = \sum_{i,j}[\mathrm{NOE}_{\mathrm{obsd}}(i) - \mathrm{NOE}_{\mathrm{calcd}}(i)]^2/\sigma^2(i) \qquad (8)$$

where $\mathrm{NOE}_{\mathrm{obsd}}(i)$ and $\mathrm{NOE}_{\mathrm{calcd}}(i)$ are the observed and the calculated NOEs for the pair of protons i and j and $\sigma(i)$ is the standard deviation of that NOE estimated from the signal-to-noise ratio on the NOE difference spectrum. The sum is taken over all intra- or internucleotide NOEs, respectively. The structural parameters which are modified during the minimization procedure are the angles defined above: pucker and glycosidic torsion angle for intranucleotide NOEs; twist, propeller twist and roll angles, and pitch for internucleotide NOEs.

For these calculations we used the correlation time that corresponds to the overall tumbling motion of the molecule: 6.4 ns at 25 °C (Lane et al., 1986a). The justification for neglecting the effect of internal motions on the correlation time in these calculations was discussed above.

It is known that in B DNA the tilt angle of the base pairs is near zero (Saenger, 1984). Since it is clear from all available data that the DNA is in the B form, variations of this angle could be neglected. The helical displacement D was kept equal to 0.17 Å. A displacement of 4 Å, characteristic of A DNA, yields a pattern and magnitudes of NOEs that are completely different from the observed ones.

Estimation of Errors. The primary source of error is the error in experimental data. The precision of the value of the NOE was taken equal to the inverse of the signal-to-noise ratio in the difference spectrum. For NOEs smaller than 0.05 the precision was only about ±50%, while for NOEs greater than 0.2 the precision was better than ±10%.

The maximum error on the structural parameters can be estimated by several approaches. The first is a nonparametric method in which the maximum errors in any parameter can be estimated from plots such as in Figure 7. For example, from graphs of intranucleotide NOEs as a function of the glycosidic torsion angle (Figure 7), the maximum range of χ can be determined from a given experimental value of the NOE and its uncertainty, for any value of the sugar pucker. In this case, the errors in χ are of the order ±3°, independent of the sugar pucker, whereas the errors in P are of the order ±32°. The uncertainty is further reduced when several NOEs are combined to determine the structural parameter.

The errors can also be esimated from the curvature matrix near the minimum of the fitting function Δ^2. The error matrix, which is the inverse of the curvature matrix (Bevington, 1969), gives the uncertainty related to each parameter on which the observed NOEs are dependent. The elements on the diagonal of the error matrix give estimates of the variance of each parameter. The off-diagonal elements give an indication of the covariance among the different parameters. Typical error matrices are given in Table VI for intranucleotide and internucleotide NOEs and related structural parameters (pucker phase and glycosidic torsion angles for the former, twist and roll angles and pitch for the latter). The uncertainties obtained from the error matrices are ±3° for the glycosidic torsion angle, ±30° for the pseudorotation phase angle, ±4° for the twist angle, ±4° for the individual base roll angle, and ±0.05 Å for the pitch.

Table VI: Comparison of the Analysis Based on the Three NOEs from H1′, H2′, and H3′ and That Using Only Two of Them (H1′ and H2′) and the Multiplicity of the H1′ Resonances from the *J*-Resolved Experiment[a]

	analysis with NOE from H1′, H2′, H3′			analysis with NOE from H1′, H2′, *J*			
base	χ (deg)	*P* (deg)	Δ^2	χ (deg)	*P* (deg)	Δ^2	*f* (%)
G2	−40	153	0.02	−38	60	0.05	0
A4	−46	127	0.13	−46	90–198	0.06	0
A7/A15	−50	60	0.12	−51	90–198	0.06	10
G8/G16	−48	66	0.03	−48	70	0.03	0
A11	−46	86	0.04	−46	126	0.13	3
A12	−43	60	0.10	−41	126	0.02	9
A18	−46	127	0.5	−47	142	0.35	0
G20	−48	159	0.63	−49	142	0.64	0

[a] χ is the glycosidic torsion angle, *P* is the phase of the pseudorotation, Δ^2 is the weighted residual, and *f* is the putative population (in %) of the opposite conformation (north or south).

Table VII: Error Matrices for Intra- and Internucleotide NOEs and Relative Structural Parameters[a]

(A) Error Matrix for G2[b]

	χ	*P*
χ	−2.3	12.1
P	12.1	−35.5

(B) Error Matrix for T6-A7[c]

	θ_T	*h*	θ_R
θ_T	−3.9	−0.14	7.9
h	−0.14	0.004	0.07
θ_R	7.9	0.07	−5.5

[a] The error matrix is obtained by inverting the curvature matrix α. The elements of the matrix a are given by $\alpha_{ij} = \partial^2\Delta^2/\partial a_i \partial a_j$, where the a_i are the different structural parameters. These parameters are indicated for rows and columns (χ, glycosidic torsion angle; *P*, pseudorotation phase angle; θ_T, twist angle; θ_R, base roll angle; *h*, pitch). The uncertainty of the parameters a_i is equal to the diagonal element α_{ii}. [b] The intranucleotide NOEs H1′ to H8 and H2′ to H8 were used to determined the function Δ^2. [c] The internucleotide NOEs T6H1′ to A7H8, T6H2′ to A7H8, T6H2″ to A7H8, and T6H6 to A7H8.

The small uncertainty of the pitch is due to the very high sensitivity of the internucleotide NOE to the inter base pair distance. On the other hand, Table VII shows that there is a substantial covariance between χ and the pucker, or between twist and roll angles, while the covariance of the pitch with the twist or the roll is very small.

(4) Trp Operator Structure

Purine Nucleotide Conformation. The NOEs to the H8 protons can be determined quite easily as these resonances are well resolved (cf. Figure 1), except for A7 and A15 at 8.18 ppm and G8 and G16 at 7.56 ppm. The chemical shifts of base and sugar protons are very similar if not identical in each pair of these nucleotides, so that A7 and A15 as well as G8 and G16 are very likely to have the same conformation. Moreover, this is expected as these nucleotides are in symmetric positions in the central region of the palindromic sequence:

-A4 - C5 - T6 - A7 - G8 - T9 -

-T17 - G16 - A15 - T14 - C13 - A12

In these two cases, the contribution of each base to the observed NOE from the deoxyribose protons (which also have similar chemical shifts) have been considered as equal. For all purines NOEs from H1′, H2′, and H3′ are available and have been used to determine the phase of the pseudorotation (pucker) and the glycosidic torsion angle. The results of this calculation are given in Table VII.

For G2, A4, G8/16, A18, and G20 the values of the residuals are acceptable, and the puckers obtained by fitting the NOEs lie in the range defined by the coupling constant between the sugar protons (Table III). These puckers and the glycosidic torsion angles were then considered valid.

For the other purines, although the residuals are reasonable, the puckers do not fall in the range determined by the spin multiplicity. If the puckers are set to the value suggested by the multiplicity, then the three NOEs cannot be satisfied at the same time. This is probably due to different effects of averaging on the coupling constants and the NOEs between several structures.

Averaging between north and south conformations of the sugar introduces more bias in the H3′–H8 NOE than in the H2′–H8 NOE, while the H1′–H8 NOE is almost insensitive to the pucker, at least within experimental error limits. In the north conformations, the NOE between H3′ and H8 is 5–10 times bigger than the NOE resulting from a south conformation, where H3′ is far from H8 (4.2 Å in C2′ endo vs. 2.8 Å in C3′ endo). Hence, even if the north conformation is a minor component (say 10%), its weight in the total NOE can be significant and can increase the apparent NOE by 50–100%. On the other hand, between the two types of conformation, the NOEs from H2′ have a typical ratio of 2. Then, 10% of a north conformation will only affect the NOE of a dominant south conformation by no more than 5%, which is less than the experimental error. We have therefore used the NOEs from H1′ and H2′ and the spin multiplicities to estimate the pucker and to calculate the glycosidic torsion angle of the most populated conformation. This gives the deoxyribose of the purines in the south conformation (essentially C2′ endo), which agrees qualitatively with the low value of the NOE from H3′.

The H3′–H8 NOE, on the other hand, gives an insight into the probable equilibrium between different states of the pucker. As we have only one experimental value for the two parameters, it is necessary to assume the nature of the alternative conformations. From the study of nucleotides in solution by NMR (Altona & Sundaralingam, 1973; Davies & Danyluk, 1974), it is reasonable to consider the C2′-endo and the C3′-endo conformations as the two states of minimum energy between which the sugars are continuously flipping. However, one should bear in mind that embedding nucleotides in a polynucleotide chain may change the position of these minima. We have discussed above that the sugar pucker cannot be accurately determined by NMR data, so that the assumption of averaging between north and south conformations is reasonable. Then the observed NOE is an average value

$$\mathrm{NOE} = \alpha_n \mathrm{NOE}_n + \alpha_s \mathrm{NOE}_s \qquad (9)$$

where $\alpha_{n,s}$ are the fractional populations in the north and the south conformations and $\mathrm{NOE}_{n,s}$ are the simulated NOEs corresponding to these individual conformations. The results presented in Table VII show that the north conformation always accounts for a minor fraction of the population (<10%). The contribution of this population to the observed NOE from H1′ and H2′ is small and in any case smaller than the experimental error. This validates a posteriori our calculation based on the H1′–H8 and H2′–H8 NOEs, ignoring the averaging effect of the minor population.

Pyrimidine Nucleotide Conformation. Table IVA indicates that, for the pyrimidines, NOE data are more scarce, so that it is not possible to evaluate the equilibrium in detail. This is due to a more extensive overlap between the resonances of the H6 protons. Reliable NOEs can still be measured when the chemical shifts of the sugar protons are sufficiently different, but it is also possible to use the NOEs to the H5 of cytosines or to the CH_3 of the thymines. Here the determination of the nucleotide conformation relies on the pucker esimated from the *J*-resolved experiment and on the NOE value from one or two of the ribose protons H1′, H2′, and also H2″. These last NOEs are relayed through the H2′ proton and can be convenient to use when two or more pyrimidines have identical H6 and H2′ frequency resonances but different H2″. Hence, in the case of pyrimidines, the available data do not allow us to investigate the averaging between different types of conformation. However, the pyrimidine H1′s show mainly doublet-splitting patterns (Table III), which indicates that these sugars are mainly in the C3′-endo conformation. The conformational parameters of the pyrimidines are given in Table VIII.

Relative Orientation of Nucleotides. Because the H8′s are well resolved, both NOEs from H1′ and H2″ are available when a purine is at the 3′ end of the dinucleotide (X-Pur type). Because of the more extensive overlap of the H6′s, more scarce NOE data are available for X-Pyr type dinucleotides (see Table IVB).

The twist angle and the 5′ base roll angle were varied for different values of the pitch to fit the NOE data in the X-Pur dinucleotides, for which enough NOE data were available. For each X-Pur dinucleotide a fit was obtained with a reasonable residual, except for T6–A7, T14–A15 (which we consider as symmetric, see above), and T17–A18. The results can be summarized in the scheme

C1 * G2 - T3 * A4 * C5 - T6 ... A7 * G8 * T9 - T10

G20 * C19 * A18...T17 * G16 * A15...T14 - C13 * A12 * A11

where the asterisk indicates that the fit using the two NOEs from H1′, H2″, and H8,6 is acceptable ($\Delta^2 < 1$), the dash shows that only one type of NOE is available for the step, and dots indicate that the fit with the two NOEs gives $\Delta^2 > 1$.

At each step except one along the sequence, the geometry of one dinucleotide (on one strand or the other) can be determined. Then, apart from the T6–A7/T14–A15 unit, all the twist angles and the pitches in the molecule are known. The remaining individual rolls for the X-Pyr dinucleotides can be determined from the internucleotide NOE that is observed in each of these dinucleotides (see Table IVB).

The inability to find a fit with an acceptable residual for T17–A18 could be attributed to a significant averaging effect in the deoxyribose of T17. The roll of T17 has been calculated by using the twist and the pitch given by the opposite dinucleotide T3–A4, and the NOE between the H1′ of T17 and the H8 of A18. This type of NOE is not very sensitive to the pucker. By simulating the H2″–H8 NOE for a south (the NOE is invariant between C1′ exo and C3′ exo) and a north (C3′ endo) conformation, it is possible to estimate that the deoxyribose of T17 is about 15% of the time in the south conformation. This distribution would give the kind of pattern observed in the 2D *J*-resolved spectrum for the T17 sugar. It is quite plausible that other purines having the same coupling constant are in the same type of equilibrium.

This equilibrium can also be invoked to explain why it is not possible to find a good fit for the step T6–A7/T14–A15.

Table VIII: Structural Parameters of the Trp Operator DNA[a]

R_1 (deg)	χ (deg)	P (deg)	B [θ_T°]	θ_p [θ_r] (deg)	B [h] (Å)	P (deg)	χ (deg)	R_2 (deg)
13	−25	S (126)	C1		G20	S (162)	−48	
			[38]	[-]	[3.4]			
−10	−38	N (60)	G2	−5	C19	N (54)	−33	5
			[34]	[−11.5]	[3.6]			
10	−33	N (54)	T3	12	A18	S (126)	−46	2
			[30]	[9.5]	[3.4]			
1	−46	S (---)	A4	13	T17	N (54)	−40	12
			[36]	[−6.5]	[3.6]			
2	−33	N (14)	C5	2	G16	N (70)	−48	0
			[43]	[−2]	[3.2]			
11	−39	N (54)	T6	16	A15	S (---)	−51	5
			[26]	[6]	[3.4]			
5	−51	S (---)	A7	16	T14	N (54)	−39	11
			[43]	[−2]	[3.2]			
1	−48	N (70)	G8	4	C13	N (45)	−25	3
			[36]	[6]	[3.6]			
−13	−35	N (20)	T9	−12	A12	S (126)	−41	1
			[44]	[−6.5]	[3.3]			
3	−35	S (---)	T10	7	A11	S (126)	−46	4
			[30]	[−1]	[3.6]			
4	−46	S (126)	A11	7	T10	S (---)	−35	3

[a] Only half of the sequence is shown as the operator is palindromic. *Parameters defining the conformation of each base pair*: χ is the glycosidic torsion angle (defined as the torsion angle of C8,6–N9–C1′–C2′) and P the phase of the pseudorotation which determine the pucker of the deoxyribose; S and N correspond to south and north conformations. The value in brackets after S or N indicates the value of P given by the calculation (P = 18: C3′ endo, P = 90: O4′ endo, P = 162: C2′ endo). (---) means that acceptable fits are obtained for all the south conformations. R_1 and R_2 are the individual base roll angles and θ_p the propeller twist angle. These angles are defined in the text. *Respective orientations between base pairs*: θ_T is the twist angle, h the local pitch, and θ_r the inter base pair roll angle calculated for each step and also reported in Figure 10.

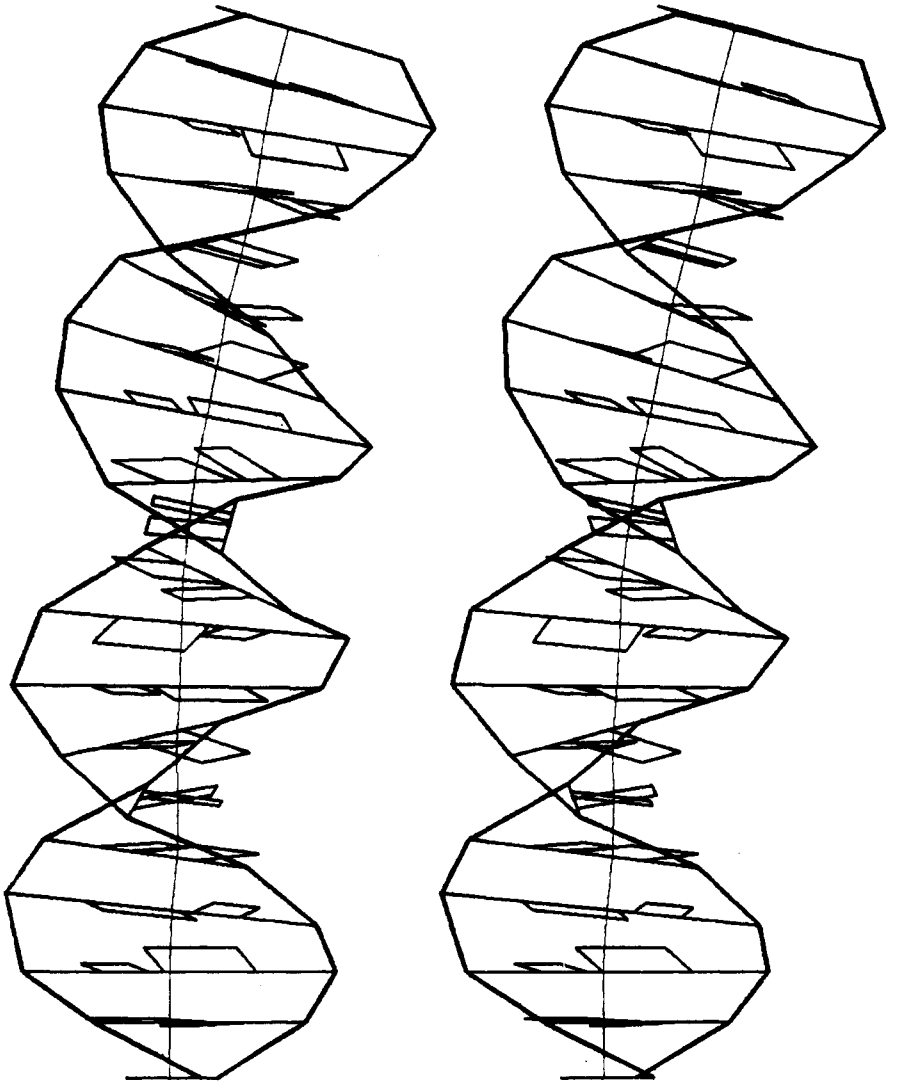

FIGURE 8: Stereoview of the model of the Trp operator structure. The construction was performed by using the data given in Table VIII. The computer graphics program was written by M. Tregger and E. Westhof according to principles described by Tung and Harvey (1986).

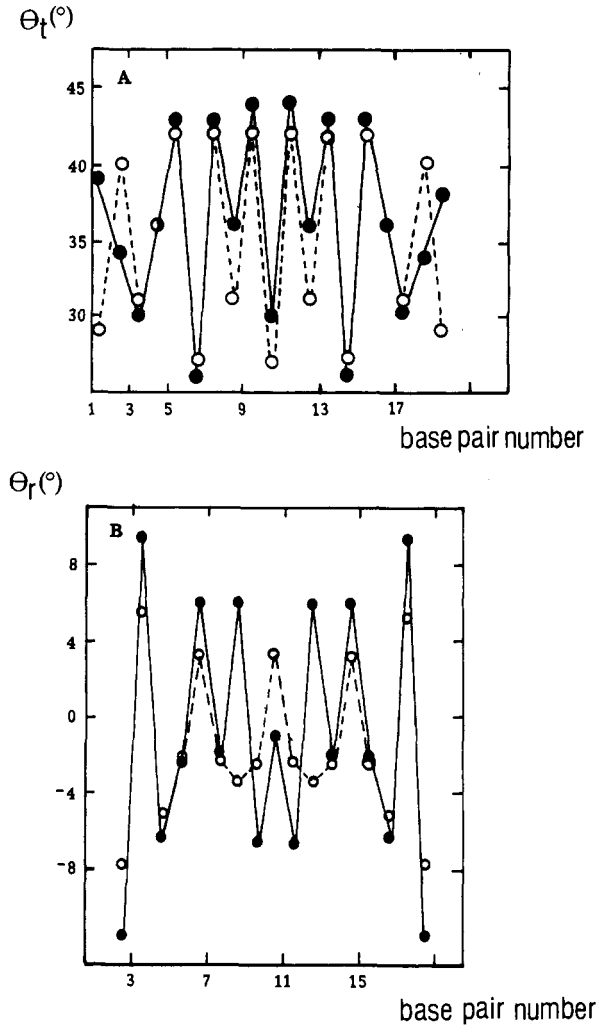

FIGURE 9: Glycosidic torsion angles as a function of puckers for purines (●) and pyrimidines (○). The line is obtained by linear regression on all points, $r = 0.75$ with $n = 18$ (C1 and G20 were not included).

There are good reasons to consider the two thymines as symmetrical as well as the two adenosines (see above). Then the NOE will be averaged in the same manner in the two opposite strands. The best estimates of the structural parameters are given in Table VIII.

A schematic drawing of the model derived from the data in Table VIII is shown in Figure 8. The drawing was computed and performed by M. Tregger and E. Westhof, according to the nucleic acid representation of Tung and Harvey (1986). Note that the conformation of the phosphate backbone is not precisely defined and therefore represented only as "a piece of string" connecting the sugar moieties. The thin line passing through the middle of the molecule is formed by the successive local helix axes. It shows that the molecule is slightly bent. The repeat of negative roll angles in the central sequence TTAA is responsible for this bend.

The NOEs have been simulated according to the method described above for the whole molecule, taking all protons into account. The spin–lattice relaxation rates, which are needed to integrate the Bloch equations, were also calculated. The reduced $\chi^2\Delta^2/N$ (where Δ^2 is defined by eq 8 and N is the number of analyzed NOEs) for the inter- and intranucleotide NOEs given in Table IV is equal to 0.7. This means that the calculated NOEs are similar to the observed, within experimental error.

Comparison with Other Known Structures. In the *Eco*RI restriction site, Fratini et al. (1982) established a correlation

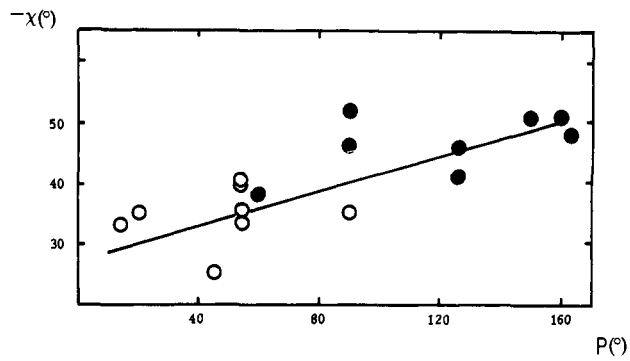

FIGURE 10: Predicted (○) and observed (●) values of twist (A) and inter base pair roll (B) as a function of sequence. The predicted values are calculated by using Calladine's rules (see text). The inter base pair roll angles are calculated from the values of the base rolls (R_1 and R_2) reported in Table VIII.

between the sugar pucker and the glycosidic torsion angle. Figure 9 shows a plot of the pseudorotation phase angle (P) against the glycosidic torsion angle (χ) for the Trp operator. The regression line (correlation coefficient $r = 0.75$) suggests that P and χ are correlated. This is probably misleading as the values taken for the pyrimidines or for the purines individually give a very poor correlation coefficient ($r = 0.19$ and 0.4, respectively). A more correct interpretation may be that the conformations of the purines are clustered around C2′ endo with larger glycosidic torsion angles, whereas the pyrimidines are characterized by a broad range of puckers near C3′ endo and have smaller glycosidic torsion angles. We note that the Trp operator contains more purine–purine or pyrimidine–pyrimidine dinucleotide motifs than the *Eco*RI site.

The mean values of the helical twist angle and the pitch found for the Trp operator are 35.5 ± 5.3° and 3.44 ± 0.16 Å, respectively. These values correspond to those of B DNA. The mean glycosidic torsion angles are −46 ± 3.8° for purines and −33.7 ± 5° for pyrimidines. This suggests that the glycosidic torsion angle is determined more by the base type than the sequence. The propeller twists of GC base pairs are small (0.33 ± 3.9°) compared with those of AT base pairs (8.7 ± 9.7°), as previously found for the *Eco*RI restriction site (Fratini et al., 1982).

Comparison with the Structure Predicted from Calladine's Rules. The observed structural variations along the operator sequence can also be predicted by using the rules of Calladine (1982) and of Dickerson (1983). Figure 10 shows the variation of the predicted twist and roll angles along with the actual values. If we ignore the first two bases, which are known to be less constrained (Dickerson, 1983), the agreement between the predicted and the calculated values of the twist angle is quite remarkable. For the roll angles, although the agreement is not as good, the trends of the calculated values agree with those predicted. The major discrepancy occurs in the central region, especially in the G8C13–T9A12 step.

We note that the same kind of agreements exist between the crystal and the predicted structure of the *Eco*RI site (Fratini et al., 1982). Calladine's predictive model was actually derived from the crystal structure of this sequence and therefore validates the model. The fact that a solution structure and a crystal structure can both be predicted in the same way by the Calladine–Dickerson rules is noteworthy.

CONCLUSIONS

By taking into account the effects of indirect magnetization transfer, we have been able to estimate several of the important structural parameters for nucleotide units in the *E. coli* Trp

operator. The structure of the Trp operator is not regular along the sequence. Some of the parameter variations that have been found, such as those of the twist angle and of the roll angle, are in agreement with the predictive model of Calladine. The precise role of these structural variations in the interaction of this oligonucleotide with proteins that recognize the sequence, such as the Trp repressor and RNA polymerase, remains to be determined.

ACKNOWLEDGMENTS

We are grateful to M. Tregger and E. Westhof for the drawing of the DNA model and to Drs. T. W.-M. Fan, P. Cruz, B. Klaič, and F. Arnold for fruitful discussions and comments. We thank J. Williamson for running the phase-sensitive NOESY spectrum.

Registry No. Operator DNA, 99637-95-3.

REFERENCES

Altona, G., & Sundaralingam, M. (1972) *J. Am. Chem. Soc. 94*, 8205–8212.

Altona, G., & Sundaralingam, M. (1973) *J. Am. Chem. Soc. 95*, 2333–2344.

Arnott, S., & Hukins, D. W. L. (1972) *Biochem. Biophys. Res. Commun. 47*, 1504–1509.

Bax, A. (1982) *Two Dimensional Nuclear Magnetic Resonance in Liquids*, D. Reidel, Dordrecht, The Netherlands.

Bevington, P. R. (1969) *Data Reduction and Error Analysis for the Physical Sciences*, Chapter 11, McGraw-Hill, New York.

Bothner-By, A. A., & Noggle, J. H. (1979) *J. Am. Chem. Soc. 101*, 5152–5155.

Braun, W., & Gō, N. (1985) *J. Mol. Biol. 186*, 611–626.

Broido, M. S., James, T. L., Zon, G., & Keepers, J. W. (1985) *Eur. J. Biochem. 150*, 117–128.

Calladine, C. R. (1982) *J. Mol. Biol. 161*, 343–352.

Calladine, C. R., & Dickerson, R. E. (1983) *J. Mol. Biol. 166*, 419–441.

Cantor, C. R., & Schimmel, P. R. (1980) *Biophysical Chemistry*, Vol. I, Chapter 4, W. H. Freeman, San Francisco.

Chazin, W. J., Wüthrich, K., Hyberts, S., Rance, M., Denny, W. A., & Leupin, W. (1986) *J. Mol. Biol. 190*, 439–453.

Clore, G. M., & Gronenborn, A. (1983) *EMBO J. 2*, 2109–2115.

Clore, G. M., Gronenborn, A. M., Moss, D. S., & Tickle, I. J. (1985) *J. Mol. Biol. 185*, 219–226.

Clore, G. M., Brünger, A. T., Karplus, M., & Gronenborn, A. M. (1986) *J. Mol. Biol. 191*, 523–551.

Davies, D. B. (1978) *Prog. Nucl. Magn. Reson. Spectrosc. 12*, 135–225.

Davies, D. B., & Danyluk, S. S. (1974) *Biochemistry 13*, 4417–4434.

Dickerson, R. E. (1983) *J. Mol. Biol. 166*, 419–441.

Fratini, A. V., Kopka, M. L., Drew, H. R., & Dickerson, R. E. (1982) *J. Biol. Chem. 257*, 14686–14707.

Gunsalus, R. P., & Yanofsky, C. (1980) *Proc. Natl. Acad. Sci. U.S.A. 77*, 7117–7121.

Hare, D. R., Wemmer, D. E., Chou, S. H., Drobny, G., & Reid, B. (1983) *J. Mol. Biol. 171*, 319–336.

Hogan, M. E., & Jardetzky, O. (1979) *Proc. Natl. Acad. Sci. U.S.A. 76*, 6341–6345.

Hogan, M. E., & Jardetzky, O. (1980) *Biochemistry 19*, 3460–3468.

Jamin, N., James, T., & Zon, G. (1985) *Eur. J. Biochem. 157*, 157–166.

Jardetzky, O., Lane, A. N., Lefèvre, J-F., Lichtarge, O., Hayes-Roth, B., & Buchanan, B. (1986) *NMR in the Life Sciences* (Bradbury, E. M., & Nicolini, C., Eds.) NATO Advanced Study Institute Series, pp 49–72, Plenum, New York.

Jeener, J., Meier, B. H., Bachmann, P., & Ernst, R. R. (1979) *J. Chem. Phys. 71*, 4546–4553.

Keepers, J. W., & James, T. L. (1984) *J. Magn. Reson. 57*, 404–426.

Keepers, J. W., Kollman, P. A., Weiner, P. K., & James, T. L. (1982) *Proc. Natl. Acad. Sci. U.S.A. 79*, 5537–5541.

Kelley, R. L., & Yanofsky, C. (1985) *Proc. Natl. Acad. Sci. U.S.A. 82*, 483–487.

Lane, A. N. (1986) *Eur. J. Biochem. 157*, 405–413.

Lane, A. N., & Jardetzky, O. (1985a) *Eur. J. Biochem. 152*, 395–404.

Lane, A. N., & Jardetzky, O. (1985b) *Eur. J. Biochem. 152*, 405–409.

Lane, A. N., & Jardetzky, O. (1985c) *Eur. J. Biochem. 152*, 411–418.

Lane, A. N., Lefèvre, J-F., & Jardetzky, O. (1986a) *J. Magn. Reson. 66*, 201–218.

Lane, A. N., Lefèvre, J-F., & Jardetzky, O. (1986b) *Biochim. Biophys. Acta 867*, 45–56.

Lefèvre, J-F., Lane, A. N., & Jardetzky, O. (1985a) *J. Mol. Biol. 185*, 689–699.

Lefèvre, J-F., Lane, A. N., & Jardetzky, O. (1985b) *FEBS Lett. 190*, 37–40.

Macura, S., Huang, Y., Suter, D., & Ernst, R. R. (1981) *J. Magn. Reson. 43*, 259–281.

Massefsky, W., Jr., & Bolton, P. (1985) *J. Magn. Reson. 65*, 526–530.

Olejniczak, E. T., Poulsen, F. M., & Dobson, C. M. (1984) *J. Magn. Reson. 59*, 518–523.

Olejniczak, E. T., Gampe, R. T., & Fesik, S. W. (1986) *J. Magn. Reson. 67*, 28–41.

Röder, O., Lüdemann, H., & von Goldammer, E. (1975) *Eur. J. Biochem. 53*, 517–524.

Saenger, W. (1984) *Principles in Nucleic Acid Structure*, Springer, New York.

Scheek, R. M., Boelens, R., Russo, N., van Boom, J. H., & Kaptein, R. (1984) *Biochemistry 23*, 1371–1376.

States, D. J., Haberkorn, R. A., & Reuben, D. J. (1982) *J. Magn. Reson. 48*, 286–292.

Tung, C. S., & Harvey, S. C. (1986) *Nucleic Acids Res. 14*, 381–387.

Wagner, G., & Wüthrich, K. (1979) *J. Magn. Reson. 33*, 675–680.

Weiss, M. A., Patel, D. J., Sauer, R. T., Karplus, M. (1984) *Proc. Natl. Acad. Sci. U.S.A. 81*, 130–134.